







# Reverse Heterojunction (Al)GaInP Solar Cells for Improved Efficiency at Concentration

Myles A. Steiner , Member, IEEE, Ryan M. France , Emmett E. Perl , Daniel J. Friedman ,  
John Simon , and John F. Geisz 

**Abstract**—Mitigating series resistance is crucial to the efficiency of concentrator solar cells at high current density. Conventional AlGaInP junction designs for the top junction of III–V multijunction cells present a challenging tradeoff between series resistance on the one hand and current collection and voltage on the other hand. In this article we discuss the physics of a reverse heterojunction solar cell that aims to improve on this tradeoff by combining a high bandgap  $\text{Al}_{0.18}\text{Ga}_{0.33}\text{In}_{0.49}\text{P}$  base and a lower bandgap (Al)GaInP emitter. The high mobility of the emitter leads to a relatively low series resistance, compared with a high bandgap homojunction cell. The electroluminescence spectrum shows emission peaks from both the emitter and base, leading to an open-circuit voltage that is not strictly dominated by either layer. The reverse heterojunction design is increasingly beneficial as the one-sun voltage increases.

**Index Terms**—Concentration, heterojunction, series resistance, III–V solar cell.

## I. INTRODUCTION

FOR MOST of the past 20 years, multijunction cells for space, concentrating photovoltaics, and hydrogen production have been based on the original GaInP/GaAs cell [1], even as they have grown to include four junctions. Recently, five- and six-junction cells have been demonstrated with the goal of further reducing the thermalization losses and boosting efficiencies to over 50% [2]. Effective utilization of the solar spectrum requires a higher bandgap top cell than 1.8-eV GaInP, and  $\sim 2.1$ -eV AlGaInP with 12%–18% aluminum content is an obvious candidate [3].

The question of how to effectively design a  $\sim 2.1$ -eV top cell for a six-junction device is not straightforward to answer. The overall performance of the cell arises from a balance between the diffusion length (photocurrent), voltage, and series resistance,

Manuscript received June 14, 2019; revised October 1, 2019; accepted November 22, 2019. This work was supported by the U.S. Department of Energy, Office of Energy Efficiency and Renewable Energy, Solar Energy Technologies Office, under agreements 30293 and 34358. (Corresponding author: Myles A. Steiner.)

M. A. Steiner, R. M. France, D. J. Friedman, J. Simon, and J. F. Geisz are with the National Renewable Energy Laboratory, Golden, CO 80401 USA (e-mail: myles.steiner@nrel.gov; ryan.france@nrel.gov; daniel.friedman@nrel.gov; john.simon@nrel.gov; john.geisz@nrel.gov).

E. E. Perl was with the National Renewable Energy Laboratory at the time of the work, and is now with Antora Energy, Berkeley, CA (e-mail: emmett@antora.energy).

Color versions of one or more of the figures in this article are available online at <http://ieeexplore.ieee.org>.

Digital Object Identifier 10.1109/JPHOTOV.2019.2957644

as well as the need to current-match the other junctions in the multijunction device. At low current densities, it is generally sufficient to maximize the current collection and voltage, but at high illumination intensities as in a concentrator photovoltaic system, the power conversion efficiency will ultimately be limited by the series resistance. Since the operating goal is, generally, to simultaneously obtain a high efficiency at a high concentration, the design must mitigate the series resistance in a way that does not significantly compromise the carrier collection or the voltage.

To appreciate the problem, let us observe that in a traditional p-n junction diode solar cell, the emitter layer is tasked with two distinct roles, not always complementary. On the one hand, the emitter forms one half of the p–n junction (the top half in III–V cells, closer to the incident light), creating an electric field that separates the electron-hole pairs. The minority carrier diffusion length,  $L_d$ , of the semiconductor is critical and must exceed the emitter thickness so that most absorbed carriers are collected. Dopants in n-type aluminum alloys tend to lead to strong deep-donor levels (DX centers) that limit the diffusion length, with the magnitude of the loss increasing with aluminum content [4]. Aluminum also getters oxygen into the semiconductor, forming a deep level trap that can further degrade the diffusion length. From the point of view of the carrier collection, AlGaInP is a more challenging material than GaInP.

On the other hand, the emitter is also required to spread the current laterally to the grid fingers so that the current can be collected by the external circuit. In this role, the carrier concentration and the majority carrier mobility are key, as a high mobility in concert with a high carrier concentration leads to a low sheet resistance,  $R_s$ . Fig. 1 shows the mobility and series resistance for a set of selenium-doped n-type  $\text{Al}_x\text{Ga}_{0.51-x}\text{In}_{0.49}\text{P}$  films, as determined by a room temperature Hall measurement. Though relatively insensitive to the carrier concentration, the mobility is a strong function of the Al composition, decreasing by a factor of two over the 0%–18% composition range.

To be specific, the sheet resistance in the emitter can be expressed as  $R_s = \frac{1}{qn\mu t}$ , where  $n$  is the carrier concentration (assumed here to be n-type),  $\mu$  is the majority carrier mobility,  $t$  is the emitter thickness, and  $q$  is the electric charge. The dependence on these parameters is illustrated in the top panel of Fig. 1. Since the x-axis is shown in units of carrier concentration ( $\text{cm}^{-3}$ ), the minority carrier diffusion length generally decreases going left to right. As shown in purple, if a high aluminum composition is required to obtain the necessary bandgap for the top cell, then increasing the carrier concentration is one way

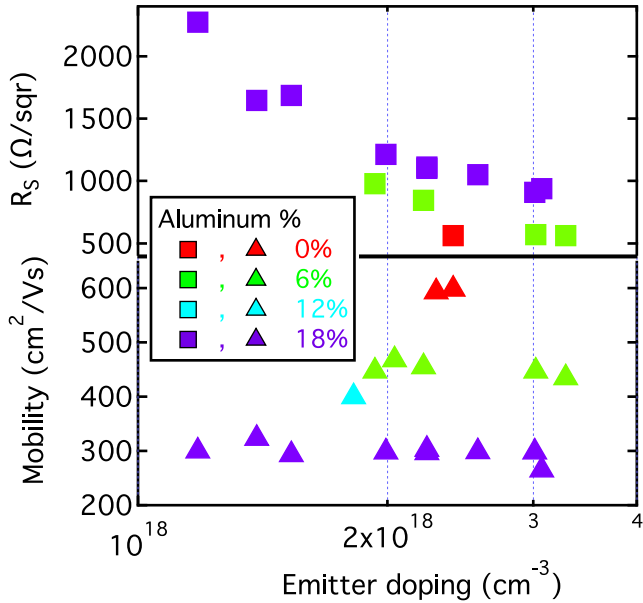


Fig. 1. Room temperature mobility and sheet resistance of selenium-doped n-type AlGaInP, as determined by a Hall measurement in a van der Pauw configuration. The Al compositions are nominal, as determined by the MOVPE reactor calibration.

to mitigate the resistance. As just noted, however, increasing the carrier concentration through heavy doping will likely also reduce the diffusion length below the emitter thickness, leading to a significant loss of carrier collection. Parasitic free-carrier absorption due to the high carrier concentration may also lead to a loss of photocurrent in the longer wavelength bottom cells of a 6J. The series resistance can also be reduced by simply increasing the emitter thickness, but a thickness that is enough to significantly lower the sheet resistance will very likely also exceed the diffusion length, thereby again ensuring a loss of carrier collection.

A different method to reduce the series resistance is to tighten the grid pitch (the spacing between adjacent grid fingers), thereby reducing the  $I^2R$  power loss due to current spreading in the emitter. But a tighter pitch comes at the expense of additional shadowing that directly reduces the photocurrent, and since the shadow loss affects every cell in the device, a tighter grid pitch also leads to an overall loss in efficiency. Transparent conductive oxides (TCOs) are sometimes used in other PV technologies to spread the current [5], but suitable TCOs that can be grown on GaAs with low Ohmic contact resistance are not readily available. Moreover, TCOs are generally not conductive enough for the high current densities of a concentrator cell nor are they sufficiently transparent over the full 350–1850 nm range of wavelengths. Thus, the standard techniques for mitigating series resistance in a planar solar cell are likely insufficient for six-junction concentrator cells.

Cell performance can sometimes be improved by raising the bandgap of the emitter to form a heterojunction, the main effect of which is to raise the voltage [6]. This strategy is effective at low concentrations, where the current density is low and the series resistance can be largely neglected, or in the second and subsequent junctions of a multijunction where current spreading

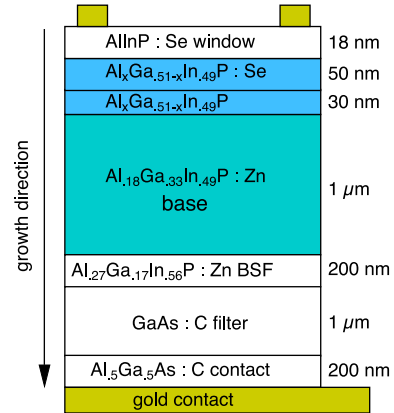


Fig. 2. Schematic of the revHJ cells, not to scale. The growth is inverted, as indicated. The nominal aluminum fraction “ $x$ ” in the emitter ranges from 0% to 18% as determined by the MOVPE reactor calibration.

can be neglected. In concentrator cells, however, the additional aluminum in the emitter will only compound the problem for the reasons already discussed.

In this article, we demonstrate another design called a “reverse heterojunction” (revHJ) cell, in which the emitter is designed with a lower bandgap than the base [7], [8]. This architecture folds together the problem of optimizing the diffusion length, series resistance, and the voltage. Using a high bandgap AlGaInP base layer and a thin, heavily doped, lower bandgap (Al)GaInP emitter layer, the cell is able to maintain a high photocurrent with a low series resistance and only suffers a minimal drop in voltage compared with a homojunction of the base alloy. As we will show, careful attention must be paid to unwanted barriers that form in the heterojunction.

## II. EXPERIMENTAL DETAILS

Cells described in this article were grown by atmospheric pressure metalorganic vapor phase epitaxy (MOVPE) on (001) GaAs substrates, miscut  $6^\circ$  toward (111)A. The cells were grown inverted and reoriented during processing. Most of the cells considered here had the structure depicted in Fig. 2. The absorber layers included a  $1\text{-}\mu\text{m}$  zinc-doped  $\text{Al}_{1.8}\text{Ga}_{3.3}\text{In}_{.49}\text{P}$  base and a 50–80 nm selenium-doped (Al)GaInP passivated emitter of varying aluminum content. The absorber was confined on the front by AllnP:Se and on the back by  $\sim\text{Al}_{2.7}\text{Ga}_{1.7}\text{In}_{.56}\text{P}:\text{Zn}$ . The GaAs back filter simulates the optical environment of the multijunction, where there is no metal reflector behind the top cell [9]. During processing, gold was electroplated to the back contact layer and the structure was bonded with epoxy to a silicon handle. The substrate was removed by wet chemical etching in ammonium hydroxide and hydrogen peroxide (1:2 by volume). Gold grids were electroplated to the front using standard photolithography, and finally, the devices were isolated using wet chemical etchants. No antireflection coatings were deposited on these cells.

We characterized our cells using standard PV techniques. Quantum efficiency was measured on a custom-built instrument using a tungsten-halogen bulb and a 0.27-m monochromator. Current–voltage (IV) curves were measured on a custom-build

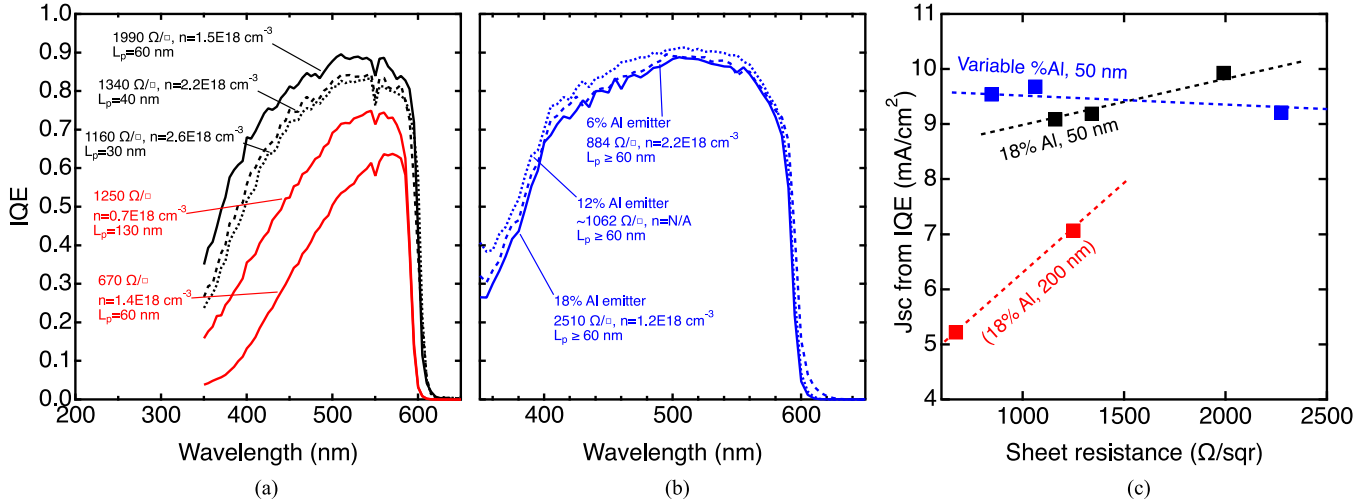


Fig. 3. (a) IQE for 18%AlGaInP homojunction cells with varying emitter doping. The emitter thicknesses are 50 nm (black curves) and 200 nm (red curves). (b) IQE for revHJ cells with 18%AlGaInP base and varying composition emitter. (c) One-sun  $J_{sc}$  as determined by integrating the IQE over the spectrum, as a function of sheet resistance. The dashed lines are guides to the eye.

solar simulator using a xenon white light source. The one-sun intensity was set using calibrated reference cells and a Spectral Evolution high-speed spectroradiometer for spectral mismatch correction [10]. Electroluminescence (EL) was measured on the same tool as the IV using the spectroradiometer to collect the emitted light. Calibration of the measurement is described elsewhere [11].

### III. EXPERIMENTAL RESULTS

#### A. Physics of the revHJ

Fig. 3 illustrates the problem with the high bandgap cells and a potential solution. The curves in Fig. 3(a) show the IQE for two sets of AlGaInP cells with 18% aluminum content, with increasing carrier concentrations in the emitter. The black curves, grown at 740 °C, had 50-nm emitters; the red curves, grown at 750 °C, had 200-nm emitters. The curves were fit to a Hovel drift-diffusion model [12] using measured carrier concentrations and dielectric constants to determine the minority carrier diffusion lengths in the emitter and base layers. The thicker emitters are more sensitive to the loss of diffusion length but the trends are the same: as the carrier concentration increases the sheet resistance decreases, but so does the diffusion length and with it the blue response of the cell.

A different trend is shown in Fig. 3(b), where the aluminum fraction of the 50-nm emitter was lowered while maintaining the 18% alloy in the base. These cells were grown at 750 °C. In this case, the blue response of the cell remains essentially constant. Fitting to the Hovel model [12] indicates that the diffusion length exceeds the emitter thickness for all three samples, though it is impossible to estimate the actual diffusion lengths in these samples. The cells were grown with the same hydrogen selenide flow rates, resulting in a carrier concentration of the 6% emitter that is  $\sim 2\times$  higher than the 18% emitter. Thus, the higher carrier concentration and higher mobility of the 6% alloy lead to a lower sheet resistance, and the blue response is still maintained.

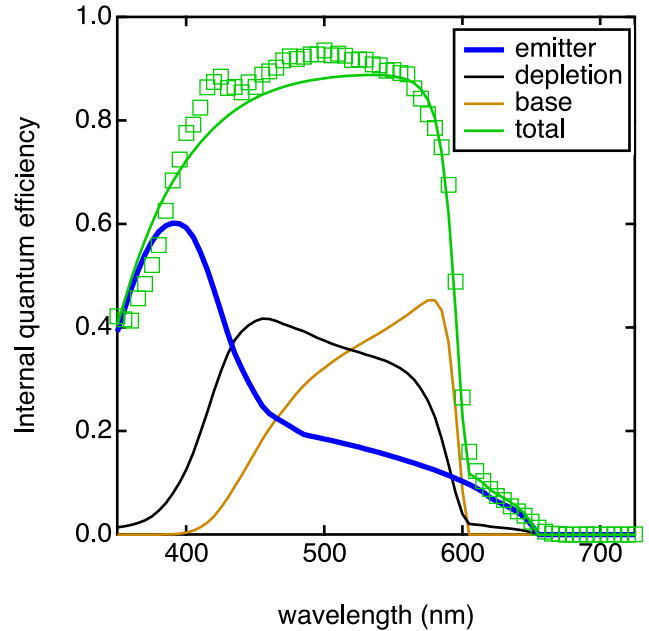


Fig. 4. IQE for a revHJ cell with a GaInP emitter and an 18%AlGaInP base, showing contributions from the emitter, depletion layer, and base. Open symbols show the measured data, solid lines show the Hovel drift-diffusion model.

These opposing trends are evident in Fig. 3(c), where the photocurrent ( $J_{sc}$ ) was estimated from the IQE by integrating over the solar spectrum. Whereas the red and black data have a positive trend (increasing  $J_{sc}$  with increasing  $R_s$ ), the blue data are relatively flat or possibly even negatively sloped, which can be attributed, in part, to the small long-wavelength tail that is visible in the dashed line in Fig. 3(b). Let us note that the two data points at highest  $R_s$  are both homojunctions with 18% aluminum, but the slightly different growth temperatures and dopant flows result in different carrier concentrations. The tail effect is more clearly seen in Fig. 4 for a different cell, with

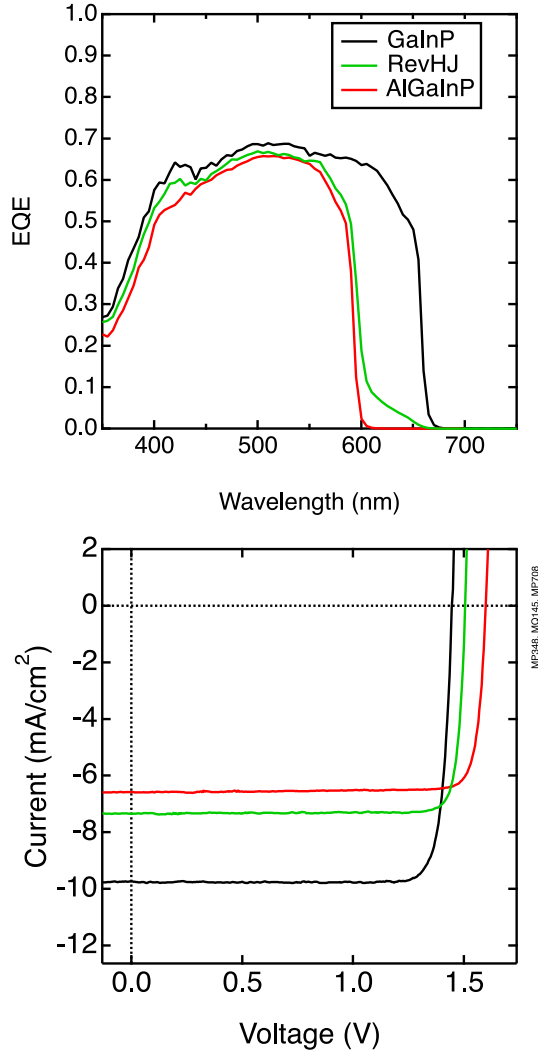


Fig. 5. (a) EQE and (b) IV curves for an 18%AlGaInP cell (red), a GaInP cell (black), and a revHJ with 18%AlGaInP base and GaInP emitter (green). IV curves were measured at  $1000 \text{ W/m}^2$ .

a  $\sim 50$ -nm GaInP emitter. Here, we have shown the individual modeled contributions of the emitter, base, and space-charge regions to the IQE. The agreement is imperfect, in part due to the limited measurements of the complex dielectric constants of the materials in the layer stack, but the model captures the essential features of the data. Both the emitter response and to a small extent the space-charge region response, extend to longer wavelengths beyond the dominant band edge of the cell. The long wavelength tail is responsible for a reduction in the cell voltage, and the questions of how much voltage is lost and whether the trade of voltage for a lower sheet resistance is beneficial are important to consider.

First, we will consider the voltage of the revHJ cell itself. Fig. 5 shows the QE and IV curves for three cells: an 18%AlGaInP cell, a GaInP cell, and a revHJ cell with a GaInP emitter and an 18%Al base. The revHJ cell has the same band edge as the AlGaInP cell but a tail that extends most of the way toward the band edge of the GaInP cell. The  $V_{oc}$  of the revHJ is somewhere between the Vocs of the homojunctions: at 1.51 V the revHJ  $V_{oc}$

is  $\sim 70$  mV above the 1.44 V for GaInP, and  $\sim 100$  mV below the 1.60 V for the AlGaInP. Thus, the revHJ cell loses some voltage but not as much as the loss in emitter bandgap.

This relative loss can be understood from the Hovel drift-diffusion model. The saturation dark current is given by

$$J_{01} = q \left( \frac{1}{N_D} \frac{D_p}{L_p} N_C N_V e^{-\frac{E_g}{kT}} \cdot \xi(p) \right)_{\text{emitter}} + q \left( \frac{1}{N_A} \frac{D_n}{L_n} N_C N_V e^{-\frac{E_g}{kT}} \cdot \xi(n) \right)_{\text{base}} \quad (1a)$$

The functions  $\xi(p)$  and  $\xi(n)$  represent the interfacial recombination at the emitter/window and base/BSF interfaces, and are given by

$$\xi(n) = \frac{(S_n L_n / D_n) + \tanh\left(\frac{x_{\text{base}}}{L_n}\right)}{(S_n L_n / D_n) \tanh\left(\frac{x_{\text{base}}}{L_n}\right) + 1} \quad (1b)$$

for the base and an equivalent formulation for  $\xi(p)$  in the emitter.  $D_n = (\mu_n kT / q)$  is the diffusion coefficient,  $L_n$  is the electron diffusion length,  $S_n$  is the surface recombination velocity,  $N_A$  is the base doping,  $x_{\text{base}}$  is the base thickness, and  $n_i^2 = N_C N_V e^{-E_g / kT}$  is the intrinsic carrier concentration. In the emitter, the subscript  $p$  indicates minority holes, and  $N_D$  is the emitter doping.  $N_c$  and  $N_v$  are calculated from the effective masses  $m_e^*$  and  $m_h^*$  as

$$N_C N_V = 4 * \left( \frac{2\pi kT}{h^2} \right)^3 (m_e^* m_h^*)^{\frac{3}{2}} \quad (2)$$

Using literature values [13] for disordered GaInP of  $m_e^* = 0.09 m_0$  and  $m_h^* = 0.7 m_0$ , where  $m_0$  is the rest mass, and  $E_g = 1.9 \text{ eV}$ , we find  $n_i \approx 275 \text{ cm}^{-3}$ . For the base we use  $N_A = 10^{17} \text{ cm}^{-3}$ ,  $L_n = 2 \mu\text{m}$ ,  $S_n \sim 1.5 \times 10^5 \text{ cm/s}$  [14], and  $\mu_n = 200 \text{ cm}^2/\text{Vs}$ , and calculate  $J_{0,\text{base}} \approx 3.1 \times 10^{-27} \text{ mA/cm}^2$ . Note that the dimensionless ratio  $S_n L_n / D_n \approx 5$  and the argument of the tanh function is approximately unity, so  $\xi(n) \approx 1.2$  and interfacial effects have only a very small effect on the calculation. For the emitter we use  $N_D = 2 \times 10^{18} \text{ cm}^{-3}$ ,  $L_n = 100 \text{ nm}$ ,  $S_n \sim 6 \times 10^4 \text{ cm/s}$  as an upper limit [14], and  $\mu_n = 20 \text{ cm}^2/\text{Vs}$ . This last number is based on the general observation that hole mobilities in III-Vs are on the order of 10 times lower than electron mobilities, though there is considerable uncertainty in the estimate. Nevertheless, we calculate  $J_{0,\text{emitter}} \approx 3.1 \times 10^{-28} \text{ mA/cm}^2$ , indicating that the dark current is dominated by the base, and we calculate  $V_{oc} = 1.44 \text{ V}$  for the GaInP homojunction at a current density of  $10 \text{ mA/cm}^2$ .

The data for AlGaInP are more sparse. Emanuelsson *et al.* [13] reported a value of  $m_e^* = 0.14 m_0$  for a 15% Al alloy. Assuming the same value of  $m_h^* = 0.7 m_0$  as for GaInP, and  $E_g = 2.1 \text{ eV}$ , we find  $n_i \approx 7.8 \text{ cm}^{-3}$ . With  $N_A = 10^{17} \text{ cm}^{-3}$ ,  $L_n = 1 \mu\text{m}$ ,  $\mu_n = 200 \text{ cm}^2/\text{Vs}$ , and using  $S_n \sim 1.5 \times 10^5 \text{ cm/s}$  as a lower limit, we again find  $\xi(n) \approx 1.2$  or slightly higher, and calculate  $V_{oc} = 1.60 \text{ V}$  for the AlGaInP homojunction.

For the RevHJ cell both terms of (1a) are important. We use the AlGaInP numbers for the base and the GaInP numbers for the emitter, and calculate that  $V_{oc} = 1.50 \text{ V}$ , in good agreement with

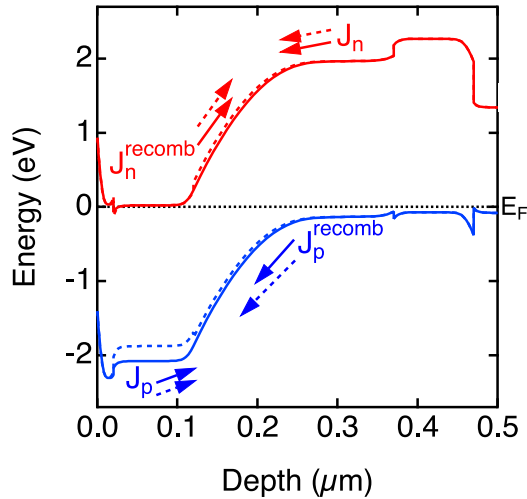


Fig. 6. Equilibrium band diagram for a 2.1-eV AlGaInP homojunction (solid) and 1.9-eV GaInP/AlGaInP reverse heterojunction (dashed) solar cell. The arrows indicate the directions and relative magnitudes of current flow. Conduction and valence band energies are shown relative to the equilibrium Fermi energy at 0 eV.

the measured data. For this revHJ cell, we estimate  $\xi(p) \approx 1.1$  in the emitter and  $\xi(n) \approx 1.2$  in the base.

Mathematically, the expression for  $J_{01}$  is not strictly dominated by the lower bandgap exponential in the emitter term—the coefficients in the two terms are sufficiently different such that the base term still has substantial weight. Physically, as illustrated in the equilibrium band diagram in Fig. 6, the lower bandgap emitter reduces the recombination barrier in the valence band but not in the conduction band, so that the total recombination is only partially reduced from the AlGaInP homojunction.

The implication in (1) that both the emitter and base contribute to the voltage and photocurrent is supported by the EL emission spectrum. Four cells were measured, shown in Fig. 7 at an injection current density of 100 mA/cm<sup>2</sup>. The black and green curves are for 18% AlGaInP and GaInP homojunctions, respectively, and show peaks at bandgaps of 2.1 and 1.9 eV, respectively. The red and blue curves are for revHJ cells with 18% AlGaInP base layers and 6% and 0% emitters. The three cells with 18% AlGaInP base layers all show emission at the base wavelength 590 nm, but with decreasing intensity as the emitter becomes less transparent with decreasing bandgap. Conversely, the emission from the emitter tracks the emitter bandgap and becomes more intense as material quality improves with decreasing Al content. The emission peaks correspond to the QE band edges and tails, as expected. It is interesting to note the slight shift in peak wavelength between the blue and green curves, and the small high-energy shoulder on the green curve. The heavy doping in the GaInP emitters of both samples likely causes kinetic disordering during growth that leads to a higher bandgap, and thus a shift in emission wavelength, relative to a more moderately doped base layer.

### B. Barriers Due to the Heterojunction

The heterojunction at the metallurgical interface between the emitter and base can cause unwanted problems if it is not

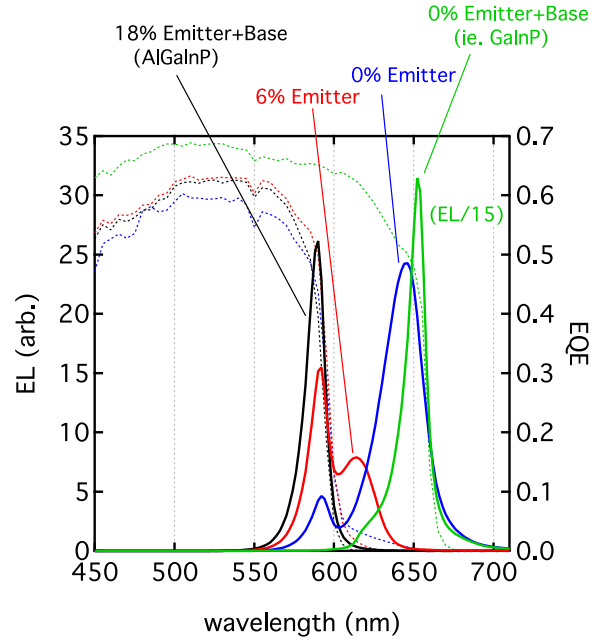


Fig. 7. EL emission from a set of homojunction and revHJ cells. The injection current was 100 mA/cm<sup>2</sup>. The measurement was calibrated as in [13]. Note the 1/15 reduced scale of the green curve. The band edge portion of the QEs (right axis) are shown as dashed lines, falling to nearly zero where the EL data peak; the tails in the blue and red QEs are observable.

managed properly. These alloys have type-I bandgap alignment, meaning that the conduction and valence bands of the wider bandgap alloy straddle those of the narrower bandgap alloy. Approximately 60% of the offset is taken up in the conduction band [15]. Referring back to the band diagram in Fig. 6, the dashed lines represent the revHJ cell and a triangular well can be seen in the space charge portion of the valence band.

To investigate the influence of the heterojunction more closely, we fabricated a GaInP revHJ cell with a GaAs emitter to exacerbate the bandgap difference. The black curve in Fig. 8(a) shows the standard QE measured at short-circuit. The QE height is very low and there is no evidence of a long-wavelength tail as would have been expected. The blue and red curves, however, show the measurement under increasing reverse bias voltage. The QE height increases significantly as the bias increases and the long wavelength tail becomes apparent. Fig. 8(b) shows the one-sun IV curve. The photocurrents at 0, -3, and -5 V match the integrated QE (i.e., integrated over the solar spectrum) at bias voltages of 0, -3, and -5 V.

Noting that the short wavelength response and long-wavelength tails both originate from the emitter, the QE response is consistent with a valence band well that is trapping minority carrier holes as they are swept by the field across the space charge region. A band diagram model for the GaAs/GaInP revHJ, similar to Fig. 6, indicates a triangular well of  $\sim 80$  Å width, which is a relatively large barrier for tunneling. Physically, as the device is reverse-biased, the bands on the n-type side (left of diagram) are pulled down relative to the bands on the p-type side (right of diagram). This does not change the height of the barrier but rather has the effect of narrowing the well and increasing the tunneling probability [16] and, therefore, the

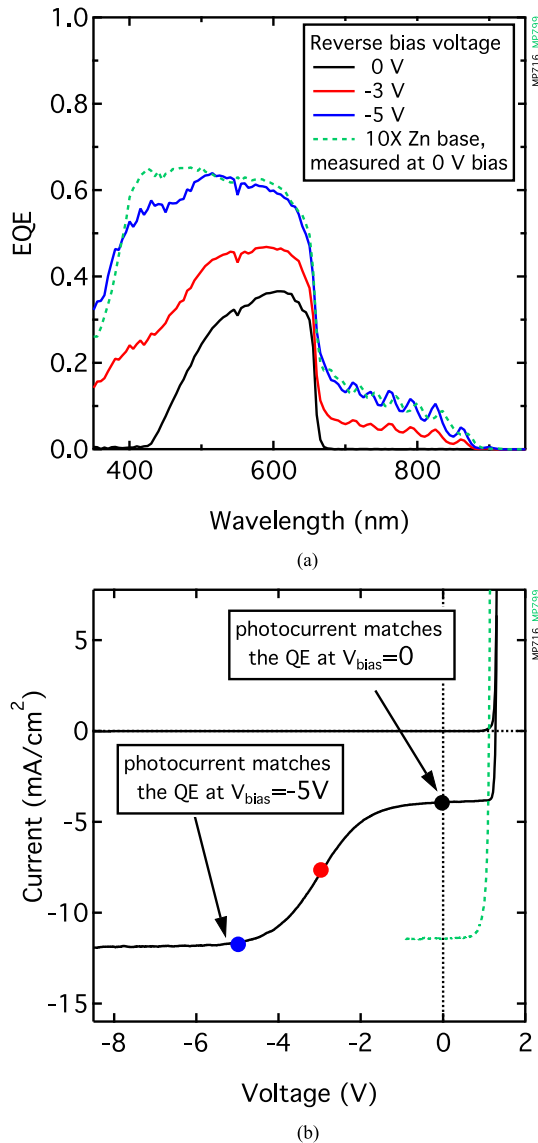


Fig. 8. (a) QE and (b) IV for a GaInP revHJ cell with a GaAs emitter. The QE curves were taken with increasing reverse bias voltage, as indicated in the legend in (a) and the colored dots in (b). The green curve shows a separate cell with  $10\times$  Zn doping in the base, measured normally.

photocurrent contribution from the emitter. Further support for this explanation is given by the green curves in Fig. 8, for a similar cell with  $10\times$  zinc doping in the base. The higher carrier concentration leads to a stronger electric field (or equivalently a steeper voltage gradient), which has the effect of narrowing the well, and QE and IV curves similar to the high reverse bias case of the first cell are observed. The valence band well is likely not as significant in an AlGaInP revHJ since the bandgaps of the two alloys are closer together than GaInP and GaAs, but a well of some width can still arise, and engineering the device to minimize the width remains important.

Another type of barrier can arise if the dopants are not properly aligned with the metallurgical junction. Fig. 9(a) and (b) shows two scenarios for the doping profile of a revHJ cell. In Fig. 9(a), the selenium n-type dopant is strictly confined to the

lower bandgap emitter region, all shown in red, and the zinc p-type dopant is strictly confined to the higher bandgap base region shown in blue. In Fig. 9(b), the n-type dopant has been allowed to extend partially into the higher bandgap base region, an effect that can occur with some MOVPE dopants due to memory effects. Equilibrium band diagrams for both scenarios are also shown, modeled with typical carrier concentrations. While the valence band well described above is apparent in the first scenario, a much larger barrier is apparent at the edge of the space charge region in the second scenario.

Fig. 9(c) and (d) shows the QE and IV for two revHJ cells with 6% AlGaInP emitters and 18% AlGaInP bases. The QE shows a decrease in both the short wavelength response and the long-wavelength tail for the cell with the barrier (red curve), consistent with an expected lower photocurrent collection from the emitter. The red IV curve is different from the one in Fig. 8, but still shows an increasing photocurrent as the cell is driven into increasing reverse bias. Let us note that in a homojunction cell there is, by definition, no metallurgical junction, and any extension of the n-type dopant into the “base region” simply increases the thickness of the emitter. This could lower the blue response of the QE if the diffusion length is not long enough. But because the depletion region is mostly on the base side of the junction, and the variation in depletion width with voltage bias is mostly taken up on the base side, the field-aided collection effect is unlikely to be significant and, therefore, the IV curve would not be expected to have a slope. Thus, the slope of the IV curve in Fig. 9(d) is indicative of a barrier.

Designing a single junction cell with a properly engineered doping profile is straightforward, as evidenced by the black curves in Fig. 9(c) and (d). However, in the context of a thick 5- or 6-junction cell that can take many hours to grow, simple diffusion of the dopants can lead to unintended barriers. The two problems—a valence band well and an emitter barrier—can be partially mitigated by growing a thicker undoped layer on the n-type side or by grading the aluminum from the lower bandgap to the higher bandgap compositions to eliminate the various wells.

#### IV. DISCUSSION

Whether or not the revHJ is beneficial amounts to balance between various power losses. Fig. 10 shows a calculation of the efficiency for concentrator cells with 1, 4, 6, and 8 junctions. The cells are simplified to a single diode model

$$J = -J_{sc} + J_0 \left( e^{\frac{q(V - J R_{eff})}{n k T}} - 1 \right) \quad (3)$$

by assuming that the total ideality factor  $n$  equals the number of junctions, and the reverse saturation current density is calculated from the total  $V_{oc}$ . Thus, for example, the 6J calculation uses a one-sun  $V_{oc} = 5.53$  V and  $J_{sc} = 8.5$  mA/cm<sup>2</sup> based on recent experimental results for a 6J [17], and is modeled with  $n = 6$  and  $J_0 = J_{sc} \exp(-\frac{qV_{oc}}{6kT}) = 2.23 \times 10^{-15}$  mA/cm<sup>2</sup>. The homojunctions have a sheet resistance of 2400  $\Omega$ /sq. The revHJs have a sheet resistance of 600  $\Omega$ /sq and a  $V_{oc}$  100 mV lower than the homojunction. These assumptions represent the 6J cells that

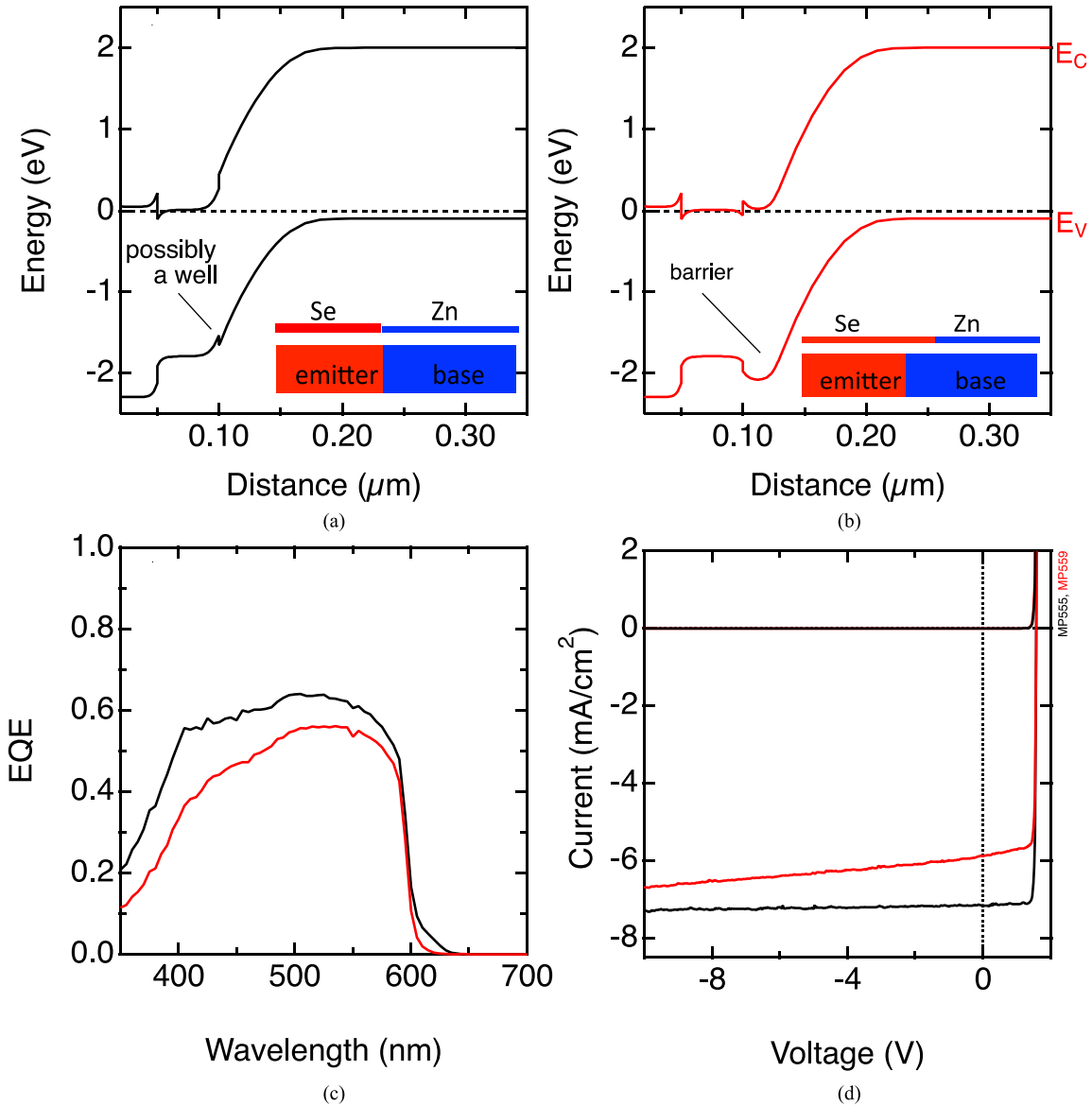


Fig. 9. Barriers in the emitter created by the doping profile. (a) Dopants properly aligned, n-type dopant in the emitter, and p-type in the base. (b) N-type dopant has diffused into the base region. For both models, the dopant profiles are illustrated in the insets. The back portions of the cell are not shown here. (c) Measured EQE and (d) measured IV curves for revHJ cells with 18%AlGaInP base and 6%AlGaInP emitter, with dopant profiles intentionally corresponding to the two models. The colors in (c) and (d) correspond to the models in (a) and (b).

we have been developing [17]. Other parameters of the model are indicated in the figure. For each point on the graph, the grid pitch was optimized so as to minimize the overall power loss [18]. The effective resistance, dominated by the sheet resistance in all cases, was included in the exponential argument of (3). The calculated shadowing fraction  $S$  was applied as a penalty on the  $J_{sc}$ , so that  $J_{sc} = J_{sc,0} (1 - S)$  where  $J_{sc,0}$  is the short circuit current density in the absence of any grids, and  $S = \text{finger width} / \text{finger spacing}$ . The fingers were assumed to be  $5 \times 5 \mu\text{m}$ .

For all four sets of modeled devices, the homojunctions (dashed lines) have a higher efficiency at low concentrations, but the curves cross so that at high concentrations the revHJ cells ultimately have a higher efficiency. The crossing point moves to lower concentration as the cell voltage increases: for the 1 J cell,

the homojunction is more efficient until  $>2000$  suns, whereas for the 6J the homojunction is more efficient until just  $\sim 260$  suns, beyond which it is slightly more beneficial to switch to the revHJ architecture.

Physically, at low concentrations the  $I^2R$  loss in the emitter is low and can be suitably managed by widely spaced grid fingers. The power loss due to shadowing is lower than the power loss due to the drop in voltage of the revHJ, so it makes sense to retain the higher voltage homojunction cell. At high concentration, the shadowing becomes large enough that the power loss due to the reduced  $J_{sc}$  exceeds the power loss due to the voltage drop, and, thus, the revHJ cell is better. As the overall voltage of the cell increases with increasing number of junctions, the relative voltage loss due to the revHJ becomes lower, and so less  $J_{sc}$  loss due to shadowing is required to make the revHJ beneficial.

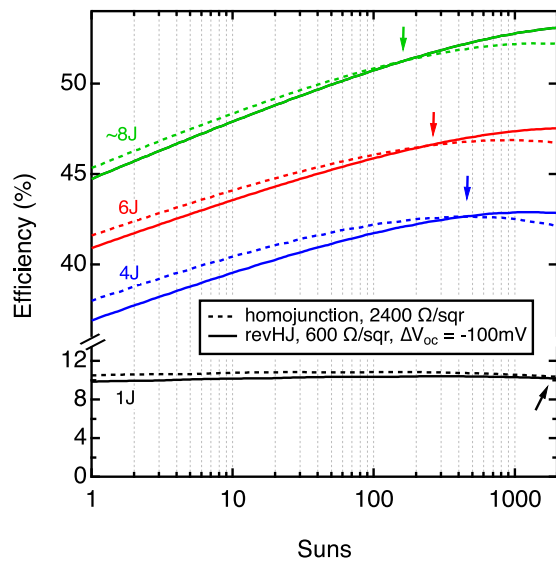


Fig. 10. Calculated efficiency for 1, 4, 6, and 8 junction solar cells, based on a simple diode model that includes resistance. The grid pitch was adjusted at each point to minimize the total power loss, which, in turn, changes the shadowing. The cells were assumed to be  $3.4 \times 3.4$  mm with two busbars; the gold grid fingers were  $5 \times 5 \mu\text{m}$  with  $2.6 \times 10^{-6} \Omega\text{-cm}$  resistivity, and the specific contact resistance was  $5 \times 10^{-5} \Omega\text{-cm}^2$ . The one-sun homojunction ( $V_{oc}$ ,  $J_{sc}$ ) values used in the model were: 1 J (1.61 V, 7.2 mA/cm<sup>2</sup>); 4 J (3.41 V, 13 mA/cm<sup>2</sup>); 6 J (5.53 V, 8.5 mA/cm<sup>2</sup>); 8 J (7.0 V, 7.5 mA/cm<sup>2</sup>) that assumes absorption out to 2500 nm. The arrows indicate the crossover between the homojunction and reverse heterojunction.

Thus, it makes intuitive sense that the crossover shifts to lower concentrations with the number of junctions.

This analysis assumes that the photocurrent of the multi-junction is affected by the grid shadowing but otherwise unaffected by the long-wavelength tail. That is clearly an oversimplification, since absorption in the tail starves the second junction of some light. If current-matching were not an issue, one could considerably thicken the GaInP emitter in Fig. 4 and significantly lower the resistance with only a slight voltage penalty. In the context of a multijunction, however, the overall efficiency would plummet as the photocurrent dropped. While the optimized selection of bandgaps and thicknesses for a 6J is beyond the scope of this article, it is important to recognize that the total absorbed photocurrent must be evenly distributed amongst the junctions and changes to the top cell cannot be considered in isolation.

Finally, Fig. 10 also shows why experimentally demonstrating the value of the revHJ can be difficult. The single-junction cells shown in Figs. 3–5 illustrate the physics of the devices, but we would still expect the efficiency of the 1 J homojunction to exceed the revHJ at all measurable concentrations.

In summary, we have shown that a top cell architecture consisting of a lower bandgap emitter and a higher bandgap base can be an effective design strategy that balances the requirements of a high photocurrent and voltage and a low series resistance. This revHJ becomes especially beneficial for high-voltage concentrator cells, where the small voltage penalty due to the lower bandgap emitter clearly outweighs the larger penalty due to shadowing that would have resulted from simply tightening the grid pitch.

## ACKNOWLEDGMENT

The authors thank W. Olavarria and M. Young for dedicated growth and processing work. This article was authored by Alliance for Sustainable Energy, LLC, the Manager and Operator of the National Renewable Energy Laboratory for the U.S. Department of Energy (DOE) under Contract DE-AC36-08GO28308. The views expressed in the article do not necessarily represent the views of the DOE or the U.S. Government. The U.S. Government retains and the publisher, by accepting the article for publication, acknowledges that the U.S. Government retains a nonexclusive, paid-up, irrevocable, worldwide license to publish or reproduce the published form of this article, or allow others to do so, for U.S. Government purposes.

## REFERENCES

- [1] J. M. Olson, A. Kibbler, and S. R. Kurtz, "GaInP<sub>2</sub>/GaAs monolithic tandem solar cells," in *Proc. 19th IEEE Photovolt. Spec. Conf.*, 1987, pp. 285–288.
- [2] J. F. Geisz *et al.*, "Building a six-junction inverted metamorphic concentrator solar cell," *J. Photovolt.*, vol. 8, no. 2, pp. 626–632, 2018.
- [3] E. E. Perl *et al.*, "Development of high-bandgap AlGaInP solar cells grown by organometallic vapor-phase epitaxy," *J. Photovolt.*, vol. 6, pp. 770–776, 2016.
- [4] S. Heckelmann, D. Lackner, C. Karcher, F. Dimroth, and A. W. Bett, "Investigations on Al<sub>x</sub>Ga<sub>1-x</sub>As solar cells grown by MOVPE," *IEEE J. Photovolt.*, vol. 5, no. 1, pp. 446–453, Jan. 2015.
- [5] M. Morales-Masis, S. D. Wolf, R. Woods-Robinson, J. W. Ager, and C. Ballif, "Transparent electrodes for efficient optoelectronics," *Adv. Electron. Mater.*, vol. 3, 2017, Art. no. 1600529.
- [6] J. M. Olson and S. R. Kurtz, "Heterojunction solar cell with passivated emitter surface," U.S. Patent 5 316 593, 1994.
- [7] R. E. Jones-Albertus and M. J. Sheldon, "Reverse heterojunctions for solar cells," U.S. Patent 9 153 724 B2, 2015.
- [8] A. B. Cornfeld, P. Patel, J. Spann, D. Aiken, and J. McCarthy, "Evolution of a 2.05 eV AlGaInP top sub-cell for 5 and 6 J-IMM applications," in *Proc. 38th IEEE Photovolt. Spec. Conf.*, 2012, vol. 38, pp. 2788–2791.
- [9] M. A. Steiner *et al.*, "Apparent bandgap shift in the internal quantum efficiency for solar cells with back reflectors," *J. Appl. Phys.*, vol. 121, 2017, Art. no. 164501.
- [10] C. R. Osterwald, "Translation of device performance measurements to reference conditions," *Solar Cells*, vol. 18, pp. 269–279, 1986.
- [11] J. F. Geisz, M. A. Steiner, I. Garcia, S. R. Kurtz, and D. J. Friedman, "Enhanced external radiative efficiency for 20.8% efficient single-junction GaInP solar cells," *Appl. Phys. Lett.*, vol. 103, 2013, Art. no. 041118.
- [12] H. J. Hovel, *Solar Cells (Semiconductors and Semimetals)*. New York, NY, USA: Academic Press, 1975.
- [13] P. Emanuelsson *et al.*, "Cyclotron resonance studies of GaInP and AlGaInP," *Appl. Phys. Lett.*, vol. 64, 1994, Art. no. 2849.
- [14] R. R. King *et al.*, "Double heterostructures for characterization of bulk lifetime and interface recombination velocity in III–V multijunction solar cells," in *Proc. 2nd World Conf. Photovolt. Energy Convers.*, Jul. 1998, pp. 86–90.
- [15] E. T. Yu, J. O. McCallin, and T. C. McGill, "Band offsets in semiconductor heterojunctions," in *Solid State Physics: Advances in Research and Applications*, H. Ehrenreich and D. Turnbull, Eds., San Diego, CA, USA: Academic, pp. 1–146, 1992.
- [16] J. R. Lang, N. G. Young, R. M. Farrell, Y.-R. Wu, and J. S. Speck, "Carrier escape mechanism dependence on barrier thickness and temperature in InGaN quantum well solar cells," *Appl. Phys. Lett.*, vol. 101, 2012, Art. no. 181105.
- [17] R. M. France *et al.*, "High efficiency 6-junction solar cells for the global and direct spectra," in *Proc. 46th IEEE Photovolt. Spec. Conf.*, 2019, to be published.
- [18] H. B. Serreze, "Optimizing solar cell performance by simultaneous consideration of grid pattern design and interconnect configuration," in *Proc. 13th IEEE Photovolt. Spec. Conf.*, 1978, pp. 609–614.